The role of sulfate groups in controlling $CaCO_3$ polymorphism

Lurdes Fernández-Díaz [a,*], Ángeles Fernández-González [b], Manuel Prieto [b]

[a] *Departamento de Cristalografía y Mineralogía, Universidad Complutense de Madrid, 28040 Madrid, Spain*
[b] *Departamento de Geología, Universidad de Oviedo, 33005 Oviedo, Spain*

Received 21 December 2009; accepted in revised form 2 August 2010; available online 14 August 2010

Abstract

The nucleation and growth of $CaCO_3$ phases from aqueous solutions with SO_4^{2-}:CO_3^{2-} ratios from 0 to 1.62 and a pH of ~10.9 were studied experimentally in batch reactors at 25 °C. The mineralogy, morphology and composition of the precipitates were characterized by X-ray diffraction, Fourier transform infrared spectroscopy, scanning electron microscopy and microanalyses. The solids recovered after short reaction times (5 min to 1 h) consisted of a mixture of calcite and vaterite, with a S content that linearly correlates with the SO_4^{2-}:CO_3^{2-} ratio in the aqueous solution. The solvent-mediated transformation of vaterite to calcite subsequently occurred. After 24 h of equilibration, calcite was the only phase present in the precipitate for aqueous solutions with SO_4^{2-}:$CO_3^{2-} \leqslant 1$. For SO_4^{2-}:$CO_3^{2-} > 1$, vaterite persisted as a major phase for a longer time (>250 h for SO_4^{2-}:$CO_3^{2-} = 1.62$). To study the role of sulfate in stabilizing vaterite, we performed a molecular simulation of the substitution of sulfate for carbonate groups into the crystal structure of vaterite, aragonite and calcite. The results obtained show that the incorporation of small amounts (<3 mole%) of sulfate is energetically favorable in the vaterite structure, unfavorable in calcite and very unfavorable in aragonite. The computer modeling provided thermodynamic information, which, combined with kinetic arguments, allowed us to put forward a plausible explanation for the observed crystallization behavior.

1. INTRODUCTION

Crystallization in the $CaCO_3$–H_2O system and the parameters that can play a significant role in controlling the formation of different polymorphs, including the development of solvent mediated transformations (Cardew and Davey, 1985) between these polymorphs, are a major topic of research in various scientific disciplines. These disciplines range from industrial crystallization (Hadiko et al., 2005; Chen et al., 2006) to biomineralization (Beniash et al., 1997; Hasse et al., 2000; Aizenberg et al., 2002, 2003; Meldrum, 2003; Weiner and Dove, 2003; Nebel and Epple, 2008; Griesshaber et al., 2009). Although calcite is its most stable polymorph under Earth's surface conditions, $CaCO_3$ can precipitate as three different crystalline forms (vaterite, aragonite and calcite), an amorphous phase (ACC) and several hydrated forms (monohydrocalcite and ikaite). The nucleation and growth of metastable $CaCO_3$ polymorphs is commonly related to the predominance of kinetic factors over thermodynamic properties (Ogino et al., 1987; Sawada, 1998). High supersaturation levels at nucleation and the initial stages of growth result in the formation of ACC, vaterite and aragonite (Sawada, 1998; Bolze et al., 2002; Pontoni et al., 2003). In agreement with Ostwald's step rule (Söhnel and Garside, 1992), these three crystalline forms ultimately transform into the more stable calcite via dissolution–crystallization reactions of various degrees of complexity (Fernández-Díaz et al., 2009). The presence of different foreign ions in the fluid during $CaCO_3$ crystallization can also promote the formation of metastable phases. For example, numerous studies have revealed that high to moderate concentrations of Mg^{2+} or Sr^{2+} in the growth medium promote the formation of aragonite instead of the more stable calcite (Reddy and Nancollas, 1976; Reddy and Wang, 1980; Lippmann, 1973). Furthermore, high Mg:Ca ratios seem to play a role in stabilizing ACC (Loste et al., 2003). There is also significant evidence that some anions, like phosphate, inhibit the formation of calcite

* Correponding author. Tel.: +34 91 3944876.
E-mail address: lfdiaz@geo.ucm.es (L. Fernández-Díaz).

(House, 1987). In fact, the presence of dissolved phosphate has been related to the formation of hydrated $CaCO_3$ ikaite ($CaCO_3 \cdot 6H_2O$) (Larsen, 1994) in natural environments where temperatures are close to 0 °C (Ito, 1996).

The role played by foreign ions in the crystallization of minerals can be a consequence of different factors, ranging from their incorporation in the structure of the crystal during the growth process, both in lattice and non-lattice positions, to their adsorption onto specific sites on crystal surfaces and to modifications of the solvent structure (Sangwal, 2007). Under high supersaturation conditions, it has been demonstrated that foreign ions can easily be incorporated into crystal structures in a higher proportion than expected from thermodynamic considerations (Chernov, 1970), especially when the incorporation of ions involves isomorphic substitutions (Fernández-Díaz et al., 1996; Prieto et al., 1997; Fernández-González et al., 2008; Katsikopoulos et al., 2009).

Dissolved sulfate is ubiquitous in sedimentary marine environments (Schulz and Zabel, 2007), and $CaCO_3$ occurrences are often associated with evaporitic environments, where the concentration of dissolved sulfate can be high (Hanor, 2004). $CaCO_3$ polymorphs formed in these environments incorporate sulfate in their structure during growth (Pingitore et al., 1995), especially when crystallization occurs under conditions that are far from equilibrium. In sedimentary carbonates, sulfate contents have been used as an indicator of diagenetic change (Land and Hoops, 1973). Furthermore, sulfate is one of the most common anions present in biomaterials like corals (Tokuyama et al., 1972) and brachiopod shells (Cusack et al., 2008). The sulfate content of biogenic calcites can be higher than 20000 ppm. In contrast, biogenic aragonite commonly has much lower sulfate levels, not exceeding 6000 ppm (Land and Hoops, 1973).

When crystal phases grow and incorporate foreign ions in their structure, their thermodynamic properties are modified. An evaluation of the changes induced in the energetics of the different $CaCO_3$ phases due to the incorporation of foreign ions into their structures would help us understand some of the complex crystallization behaviors reported in the $CaCO_3$–H_2O system (Larsen, 1994; Ito, 1996; Kitamura, 2002). However, direct measurements of thermodynamic properties are difficult, especially when relatively small differences are involved. In such cases, molecular simulation methods can be useful tools for providing accurate information about the extent of ionic substitutions and how these substitutions modify the energetics of a crystal structure. Moreover, when several polymorphic forms exist, the information provided by computational methods on the change of the thermodynamic properties of each polymorph is a useful clue to interpret the formation of unexpected phases.

This work aims to improve our understanding of the effect of sulfate ions in the growth medium on the formation of the $CaCO_3$ polymorphs calcite, aragonite and vaterite. This work also provides thermodynamic arguments that, combined with kinetic factors, help explain the crystallization behavior observed. To achieve these goals, we carried out two types of studies. First, we performed standard room temperature precipitation experiments by mixing $CaCl_2$ and $Na_2CO_3 + Na_2SO_4$ solutions, varying the SO_4^{2-}:CO_3^{2-} ratio while constantly maintaining the initial supersaturation with respect to the $CaCO_3$ phases. The precipitates were aged in contact with the parental solution during various periods of time. This action was performed to distinguish the specific influence of dissolved sulfate on the mineral composition of the precipitate from the kinetic effect of the high supersaturation prevailing in the system during the very initial stages of the crystallization. Second, we performed a molecular simulation study of the effect that the substitution of small amounts of carbonate groups by sulfate groups has on the relative energies of the crystalline structures of vaterite, aragonite and calcite. The results allow us to explain the differences in mineral composition of the experimental precipitates and to relate these differences to both kinetic and thermodynamic factors.

2. EXPERIMENTAL METHODS

2.1. Precipitation experiments

To obtain a $CaCO_3$ precipitate from solutions of various SO_4^{2-}:CO_3^{2-} molar ratios, 100 ml of a $CaCl_2$ solution were added to polypropylene vessels containing 100 ml of continuously stirred solutions of $Na_2CO_3 + Na_2SO_4$. The reactors were immediately sealed with a cover and maintained in a temperature controlled (25 ± 0.5 °C) laboratory cabinet. All of the solutions were prepared with 18 MΩ Milli-Q grade water. The initial saturation indices (SI) of the solutions with respect to the three $CaCO_3$ polymorphs were calculated using the expression:

$$SI = \log(\Omega) = \log IAP/K_{sp}, \quad (1)$$

where IAP stands for the product of ion activities in the aqueous solution raised to their stoichiometric coefficients in the solid formula; K_{sp} stands for the thermodynamic solubility product of the solid phase; Ω is the saturation state; $SI = 0$ reflects equilibrium; values of $SI < 0$ correspond to undersaturation; and values of $SI > 0$ mean that the system is supersaturated with respect to the solid considered. The calculation of SI was performed using PHREEQC (Parkhurst and Appelo, 1999), and the phreeqc.dat database was completed with the solubility product of vaterite ($10^{-7.91}$; Plummer and Busenberg, 1982). The concentration of the reactant solutions and the initial SO_4^{2-}:CO_3^{2-} ratio, the calculated pH, and the saturation index with respect to calcite in the mixed solutions are shown in Table 1. As can be seen, the initial SI values in all the experimental solutions are extremely high and nearly identical. Nevertheless, the solutions were always undersaturated with respect to both gypsum and anhydrite. It is worth noting that the SI values compiled in Table 1 represent the "nominal" initial supersaturation that could be achieved in the system before nucleation. In practice, given that a short induction period is to be expected, the rate of crystallization will probably exceed the mixing velocity, so that the actual SI will be limited by crystal precipitation (e.g., Söhnel and Mullin, 1987; Kile et al., 2000; Kowacz et al., 2010). As a result, the first nucleating particles will grow while more

Table 1
Summary of the initial fluid chemistry.

Exp	Solution composition (mol/kg)				Relevant dissolved species (mol/kg)					
	Na_2CO_3	Na_2SO_4	$CaCl_2$	$pH_{calculated}$	$[CO_3^{2-}]$	$[SO_4^{2-}]$	$[Ca^{2-}]$	$SI_{calcite}$	SI_{Gypsum}	SO_4^{2-}/CO_3^{2-}
E0	0.050	0	0.050	10.91	0.01012	0	0.01715	3.78		0
E1	0.050	0.003	0.050	10.91	0.01031	0.001989	0.01702	3.78	−0.86	0.19
E2	0.050	0.005	0.050	10.91	0.01043	0.003325	0.01694	3.77	−0.65	0.32
E3	0.050	0.010	0.050	10.91	0.01071	0.006692	0.01679	3.76	−0.37	0.63
E4	0.048	0.012	0.049	10.91	0.01032	0.008045	0.0167	3.74	−0.29	0.78
E5	0.046	0.014	0.049	10.89	0.009757	0.009346	0.01722	3.73	−0.22	0.96
E6	0.044	0.016	0.049	10.88	0.009204	0.01064	0.01775	3.71	−0.15	1.16
E7	0.042	0.018	0.049	10.86	0.008666	0.01191	0.01829	3.7	−0.09	1.37
E8	0.040	0.020	0.049	10.85	0.008141	0.01318	0.01884	3.68	−0.04	1.62

nuclei are simultaneously generated, which will affect the crystal size distribution (CSD) and induce a certain degree of compositional heterogeneity (see Section 3.1) in the solids.

For each SO_4^{2-}:CO_3^{2-} ratio, several independent runs were conducted. The experiment was terminated and the solids were sampled after increasing reaction times (5 min and 1, 24, 70, 120, 250 and 340 h). The solids were separated from the solution by filtration through a 0.45-μm membrane and washed three times with Milli-Q water to remove excess salts that could interfere with their chemical characterization. The total volume of Milli-Q water used was 15 ml. The solids were subsequently rinsed with 10 ml of ethanol and dried in a drying chamber at 30 °C. The complete set of experiments is summarized in Table 2.

2.2. Precipitate characterization

The mineralogy of the filtered solid phases was identified by X-ray powder diffraction (XRD) using a Panalytical X'Pert PRO MRD microprocessor-controlled X-ray diffractometer. This diffractometer had a Cu K_α radiation source, a primary monochromator and an RTMS detector, and was operated at 45 kV and 40 mA. Scans were recorded between 10° and 80°, with a step size of 0.0334° and an effective counting time of 200 s. Diffraction patterns were compared to standard mineral files compiled in the ICDD-PDF2 database (released 2007). A semi-quantitative estimate of the percentage of the different crystalline solids forming the precipitates was performed using the Reference Intensity Ratio (RIR) method (Snyder, 1992) while considering the RIR values included in the PDF cards (01-071-3699 for calcite and 01-074-1867 for vaterite). In all cases, triplicate runs of the experiments yielded similar results (<5% difference in the phase percentage). The characteristics of the filtered solid were further studied by Fourier transform infrared (FTIR) spectroscopy. The FTIR spectra of the samples diluted in KBr were obtained using a BRUKER IFS 66v/S spectrophotometer equipped with a TGS detector. Each spectrum was recorded by the co-addition of 64 scans. Under the conditions used, the precision was 0.2 cm^{-1}. Finally, the composition of the solids was analyzed using a JEOL JSM 6400 Scanning Electron Microscope (SEM), equipped with an Oxford Instrument Energy Dispersive X-ray (EDX) detector.

2.3. Computational methods

To evaluate the effects of the incorporation of small amounts of sulfate ions on the structure and stability of the $CaCO_3$ polymorphs, atomistic simulation modeling techniques were applied. The potential model used for energy minimization is based on the Born model of solids (Born and Huang, 1954), which assumes that the ions in a crystal interact via long-range electrostatic forces and short-range forces (Van der Waals attractions and repulsions). These interactions are described using simple analytical functions. The force field of a system consists of the set of charges and functional parameters required to describe all the interactions between the participating species. In the present work, a set of data was derived from the force fields given by Rohl et al. (2003) and Allan et al. (1993). The force field provided by Rohl et al. (2003) was originally developed to model calcium carbonate, whereas the force

Table 2
Mineral identity of the solid phases recovered in each experiment after different reaction times.

Exp	SO_4^{2-}/CO_3^{2-}	5 min	1 h	24 h	70 h	120 h	250 h
E0	0	calcite + vaterite	calcite + vaterite	calcite			
E1	0.19	calcite + vaterite	calcite + vaterite	calcite			
E2	0.32	calcite + vaterite	calcite + vaterite	calcite			
E3	0.63	calcite + vaterite	calcite + vaterite	calcite			
E4	0.78	calcite + vaterite	calcite + vaterite	calcite			
E5	0.96	calcite + vaterite	calcite + vaterite	calcite			
E6	1.16	calcite + vaterite	calcite + vaterite	calcite + vaterite	calcite + vaterite	calcite	
E7	1.37	calcite + vaterite	calcite + vaterite	calcite + vaterite	calcite + vaterite	calcite + vaterite	calcite
E8	1.62	calcite + vaterite	calcite + vaterite	calcite + vaterite	calcite + vaterite	calcite + vaterite	calcite + vaterite

field provided by Allan et al. (1993) was derived for a range of sulfates, including calcium sulfate. The quality and transferability of both force fields are supported by their excellent performance in the simulation of a wide range of properties, including bulk properties, surface energies and structures (Bruno et al., 2008), morphologies (Titiloye et al., 1993, 1998), surface–water molecule interactions (Adam, 2003), defects (Smith et al., 2006), and anionic and cationic substitutions (Becker et al., 2006; Prieto et al., 2000). These two sets of potentials had to be completed by adding a new term to the force field to describe the short-range interaction between the oxygens of the CO_3^{2-} (O_C) group and those of the SO_4^{2-} (O_S) group. The expression that describes this interaction was expressly developed for this work by fitting the O_C–O_S interaction in the crystal structure of the mineral burkeite, $Na_6CO_3(SO_4)_2$, to a Buckingham potential. The crystal structure of this mineral is especially suitable for this work because it includes both CO_3^{2-} and SO_4^{2-} anionic groups (Giuseppetti et al., 1998). The degree of agreement between the experimental and calculated structures of burkeite was above 95%. The whole force field used in the present work, including this new parameter, is shown in Table 3.

A series of super-cells was built for each polymorph. The number of $CaCO_3$ formulae per super-cell ranged from 18 to 256. In each super-cell, one of the CO_3^{2-} groups was substituted by an SO_4^{2-} group. Due to the different $CaCO_3$ formula contents of the unit cell of the three $CaCO_3$ polymorphs studied, the range of CO_3^{2-}–SO_4^{2-} substitution considered in each particular case varied. The resulting doped super-cells were optimized at constant pressure, and their energies were calculated. Moreover, the final relaxed structures were constructed and compared with the corresponding relaxed pure phases. For each configuration, more than five different initial random orientations of the sulfate molecule were considered. These orientations were selected with the help of the random number generator algorithm described by Park and Miller (1988). All of the calculations were carried out using the GULP program (Gale, 1997; Gale and Rohl, 2003). This program is a utility for the symmetry-adapted simulation of solids, it is able to treat systems of all dimensionalities from 0- to 3-D and can work with different potential models. The graphical representation of the structures was carried out using Gdis (Fleming and Rohl, 2005), a program for the visualization of molecular and periodic systems.

The initial crystal structures of calcite ($R\bar{3}c$) and aragonite (*Pmcn*) used to build the super-cells of different composition were taken from Graf (1961) and de Villiers (1971), respectively. In the case of vaterite, two different strategies were adopted. In the first strategy, the orthorhombic (*Pbmn*) crystal structure proposed by Meyer (1960) was used. This crystal structure does not allow the structural disorder of the CO_3^{2-} groups, which simplifies the simulation (de Leeuw and Parker, 1998; Medeiros et al., 2007). In the second strategy, the hexagonal $P6_3/mmc$ crystal structure given by Kamhi (1963) was used. In this crystal structure, the carbonate groups are randomly disposed among three orientations. In the present work, each of the three orientations was modeled separately and the results averaged.

3. RESULTS AND DISCUSSION

3.1. Precipitation experiments

The mineralogical composition of the precipitate recovered in each run is presented in Table 2. The XRD analyses show that the mineralogical composition of the samples varied as a function of both the initial SO_4^{2-}:CO_3^{2-} ratio in the aqueous solution and the time elapsed between reactant mixing and precipitate filtration. The SEM images in Fig. 1 illustrate the influence of both the SO_4^{2-}:CO_3^{2-} ratio in the solution and the reaction time on the precipitate morphologies. In the absence of sulfate in the solution (E0 in Tables 1 and 2), the precipitate sampled 5 min after the solutions were mixed consisted of calcite and vaterite crystals. An identical mineral composition was found after 1 h of equilibration in the parental solution (Fig. 1a). However, after one day of ageing, the precipitate exclusively consisted of calcite (Fig. 1b). In experiments E1–E5 (Table 1 and 2), in which the fluid had $0.19 < SO_4^{2-}:CO_3^{2-} \leqslant 1$, the evolution of the precipitate mineralogy was identical to that described for experiment E0. The precipitates recovered after 5 min and 1 h consisted of a mixture of calcite and vaterite, whereas calcite was the only polymorph present 24 h after reagent mixing. In contrast, in the experiments performed using solutions with $SO_4^{2-}:CO_3^{2-} > 1$ (E6–E8), the precipitate mineralogy evolved differently for longer reaction times. As can be seen in Table 2, 24 h after the beginning of the experiment, the precipitate still consisted of a mixture of calcite and vaterite in experiments E6–E8, with vaterite as the major phase (~80%) (Fig. 1c and e). After 70 h, vaterite still made up a significant proportion (~16%) of the precipitate in E6 ($SO_4^{2-}:CO_3^{2-} = 1.16$), and it represented ~45% of the precipitate in E8 ($SO_4^{2-}:CO_3^{2-} = 1.62$) (Fig. 1f). Finally, after 250 h, vaterite was only detected in the precipitate of experiment E8. In this last case, although vaterite was present in a small proportion (~5%), its crystals were still clearly distinguishable by SEM. The bar plots in Fig. 2 illustrate the phase distribution of the precipitates as a function of the initial $SO_4^{2-}:CO_3^{2-}$ ratio (after 5 min – Fig. 2a – and 24 h – Fig. 2b – of reaction) and as a function of the reaction time for the $SO_4^{2-}:CO_3^{2}$ ratio in E8 (Fig. 2c). The X-ray diffraction patterns in Fig. 3 show the mineralogical evolution of the solids recovered from the subsequent runs of experiment E8. As can be observed, the relative intensity of the reflections corresponding to calcite and vaterite evolved with the reaction time. The diffractograms show well-defined reflections in the case of calcite, whereas the reflections corresponding to vaterite show some peak broadening. This broadening was most likely due to a small crystallite size (the size of the coherently diffracting domain) than to compositional heterogeneity. In fact, the compositional ranges involved, as will be explained below, were not wide enough to produce significant peak broadening. Note that while calcite particles consisted of rhombohedra with edges >10 μm, the vaterite particles were spherulites ($Ø \approx 10$–2 μm) formed by the aggregation of very small individual crystals. Each one of these crystals may have consisted of several smaller diffraction domains.

Table 3
Force field parameters used in the computer simulations.

Atom 1	Atom 2	Atom 3	Atom 4	A eV	B Å	C eV Å^6	D_e eV	a_0 Å^{-1}	r_0 Å	k_θ eV/rad^2	θ (°)	k_2 eV Å^{-2}	K_4 eV Å^{-4}	k_{cs} eV Å^{-2}	Cutoff Å
Buckingham potentials: $E(r) = \mathrm{A}\exp(-r/B) - C/r^6$															
O_C core	O_C core			4030.3	0.245497	0.0									Intra/2.5
O_C shell	O_C shell			64242.454	0.198913	21.8436									Inter/15.0
Ca core	O_C shell			2154.0	0.289118	0.0									10.0
Ca core	C core			$1.2x10^8$	0.120	0.0									10.0
O_S core	O_S core			103585.02	0.200	25.9800									10.0
Ca core	O_S core			1651.35	0.2931	0.0									10.0
O_C shell	O_S core			100180.0	0.2147	25.99									Inter/15.0
Morse potentials: $E(r) = D_e(\{1-\exp[a_0(r-r_0)]\}^2-1)$															
C core	O_C core						5.0	2.5228	1.19820						Bonded
S core	O_S core						5.0	1.2	1.505						Bonded
Three-body potentials: $E(r) = 0.5\,k_\theta(\theta-\theta_0)^2$															
C core	O_C core	O_C core								1.7995	120.0				Bonded
S core	O_S core	O_S core								15.0	109.47				Bonded
Out of plane potential: $E(r) = k_2{}^2 + k_4 d^4$															
C core	O_C core	O_C core	O_C core									8.6892	360.0		Bonded
Spring potential: $E(r) = 0.5K_{cs}r^2$															
O_C core	O_C shel													52.740087	0.8

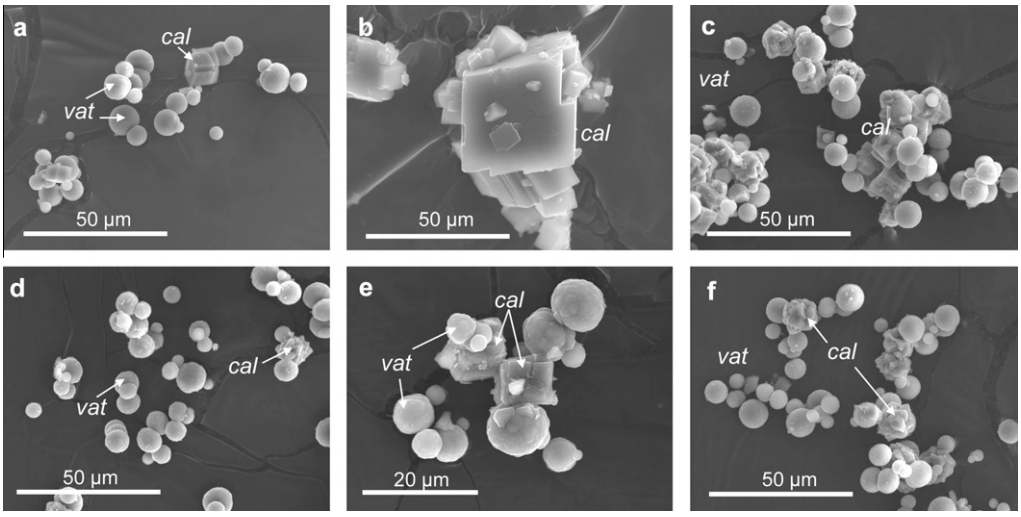

Fig. 1. SEM images of precipitates recovered from solutions with different SO_4^{2-}:CO_3^{2-} ratios after various elapsed times: (a) E0, SO_4^{2-}:CO_3^{2-} = 0, elapsed time = 1 h; (b) E0, SO_4^{2-}/CO_3^{2-} = 0, elapsed time = 24 h; (c) E6, SO_4^{2-}/CO_3^{2-} = 1.16, elapsed time = 24 h; (d) E8, SO_4^{2-}/CO_3^{2-} = 1.62, elapsed time = 1 h; (e) E8, SO_4^{2-}/CO_3^{2-} = 1.62, elapsed time = 24 h; (f) E8, SO_4^{2-}/CO_3^{2-} = 1.62, elapsed time = 70 h. Vaterite (*vat*) crystals appear as rough spheres, and calcite (*cal*) crystals show the typical rhombohedron shape. For identical elapsed times, higher concentrations of sulfate correlate with smaller and less idiomorphic calcite crystals.

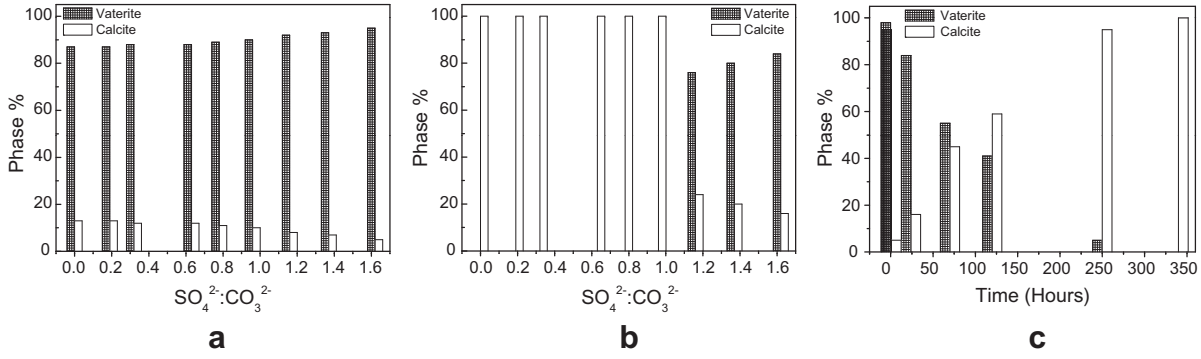

Fig. 2. Percentages of calcite and vaterite, plotted as a function of the SO_4^{2-}:CO_3^{2-} mole ratio in the parental solution after (a) 5 min and (b) 24 h interaction. In (c) this percentage is represented as a function of time for precipitates formed from solutions with an initial SO_4^{2-}:CO_3^{2-} mole ratio of 1.62 (E8).

The SEM micrographs show that the presence of dissolved sulfate in the parental solution strongly affected the size of the particles, which, for identical reaction times, decreased in size as the relative sulfate concentration was increased. Furthermore, the SO_4^{2-}:CO_3^{2-} ratio in the solution also affected the morphology of the calcite crystals, which were single crystals with the typical rhombohedral shape when the ratio was low, but progressively became blockier as the concentration of sulfate in the solution increased. Compare, for example, the calcite crystals in images b, c and e in Fig. 1, all of which reacted for 24 h. The calcite crystal in image b, which was grown in the absence of dissolved sulfate (E0), was more idiomorphic and considerably larger than the crystals in images c and e, which were grown from solutions with SO_4^{2-}:CO_3^{2-} ratios of 1.16 (E6) and 1.62 (E8), respectively.

The EDX microanalyses conducted on the precipitates recovered after a 5-min reaction time indicate that all of the solids contained S except those recovered from E0, which formed in the absence of dissolved sulfate. Moreover, there is a clear correlation between the amount of S detected in the solids and the SO_4^{2-}:CO_3^{2-} ratio in the solution. This correlation is shown in Fig. 4, where the average S:Ca mole ratios measured in the vaterite and calcite crystals are plotted against the initial parental solution SO_4^{2-}:CO_3^{2-} ratio. The S:Ca mole ratios reported for calcite and vaterite are the average of 10 measurements, and the error bars represent the standard deviation with respect to the mean value. As can be seen, the S:Ca ratio in all cases, which is equivalent to the molar fraction of sulfate, was always higher in calcite than in vaterite. Moreover, the difference in S content between calcite and vaterite increased with the initial SO_4^{2-}:CO_3^{2-} ratio in the aqueous solution. The higher S content of calcite was most likely a consequence of this phase forming later than vaterite. Because the early precipitation of vaterite would necessarily

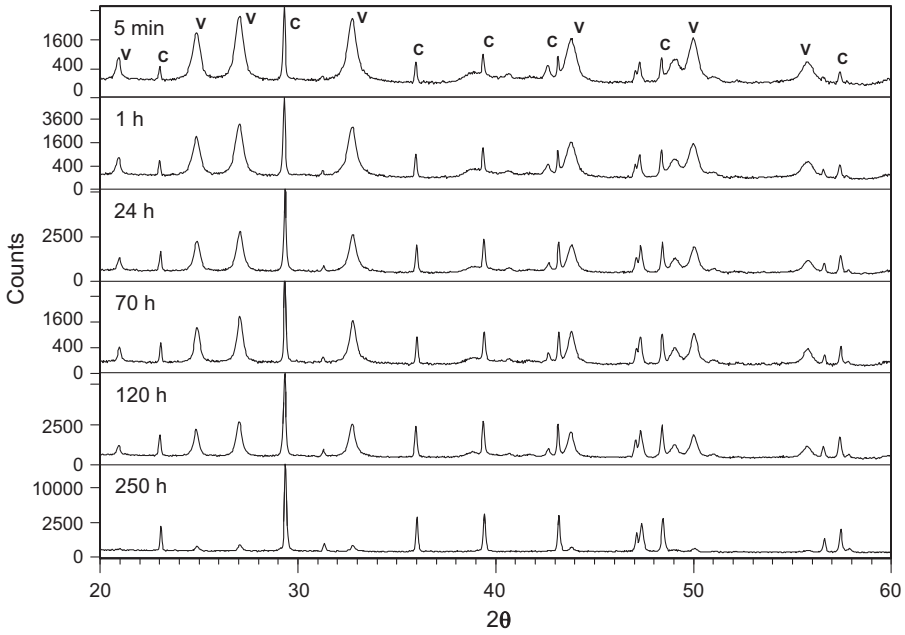

Fig. 3. XRD patterns of precipitates obtained from an aqueous solution with an SO_4^{2-}:CO_3^{2-} ratio of 1.62 (E8) as a function of time. *C* stands for calcite and *V* stands for vaterite.

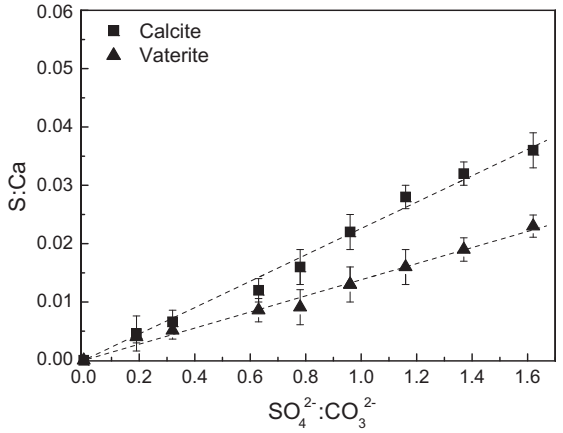

Fig. 4. S:Ca mole ratios in calcite and vaterite crystals sampled after 5 min of reaction as a function of the initial SO_4^{2-}:CO_3^{2-} mole ratio in the fluid. The data-points represent the average of 10 EDX microanalyses. Crystal morphology was used as a criterion to distinguish the mineral phase.

deplete the solution in CO_3^{2-}, calcite crystals forming thereafter would grow from a medium with a significantly higher SO_4^{2-}:CO_3^{2-} ratio than the initial solution. This higher ratio would then be reflected in the composition of the calcite.

Though the initial crystals had some compositional heterogeneity (see error bars in Fig. 4), they did not exceed a 10% S:Ca ratio for compositions measured after 5 min of reaction. This heterogeneity can be ascribed to a crystallization rate that was faster than the mixing rate of the reactants, as indicated in section 2.1. The possible compositional evolution of the precipitate during the subsequent dissolution–recrystallization process is related to a different mechanism. Upon ageing, the average S:Ca ratio in calcite decreased from ~0.04 (5 min) to ~0.02 (250 h) in experiment E8. Accordingly, the SO_4^{2-} concentration in the aqueous solution should increase with ageing of the precipitates. An in-depth study of the complex phenomenon of the redistribution of sulfate between the aqueous solution and the solid phases is, however, beyond the scope of this paper and will be addressed in future work.

To further characterize the precipitates, FTIR spectroscopic analyses were performed. All of the IR spectra showed absorbance bands characteristic of vaterite and/or calcite, but the presence of aragonite was not detected in any sample, in agreement with the XRD analysis results. Fig. 5 shows the relevant regions of the IR spectra of precipitates recovered from experiments E0, E5, and E8 after 1 h of reaction. The assignments of bands to the different vibrational modes of the carbonate ion in calcite and vaterite are indicated. The in-plane bending bands (ν_4) at 713 and 745 cm^{-1}, respectively, are characteristic of calcite and vaterite (Vagenas et al., 2003). Most significant is the presence in spectra E5 and E8 of a weak band at around 1130 cm^{-1} and three very weak and broad bands at around 670, 628 and 608 cm^{-1}, which are absent in spectrum E0. These bands occur at wavelengths consistent with the positions of the ν_3 antisymmetric stretch and the ν_4 antisymmetric bending vibrations of the sulfate tetrahedra in minerals, which occur between 1180 and 1030 cm^{-1} (stronger bands, ν_3) and around 670–580 cm^{-1} (weaker bands, ν_4) (Bensted, 1976; Farmer, 1974). The absence of these bands in the solids formed from a sulfate-free solution (E0), together with their stronger intensity in the solids formed from solutions of increasing SO_4^{2-}:CO_3^{2-} ratios support this interpretation.

Our findings indicate that the mineral composition of the precipitates is determined by two factors: the high

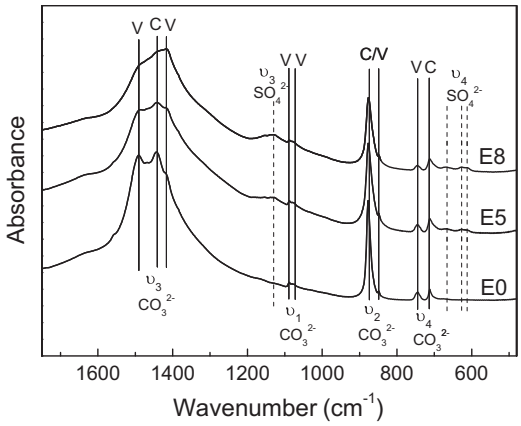

Fig. 5. Infrared spectra of precipitates sampled after 1 h of reaction in the case of experiments E0 (SO_4^{2-}:CO_3^{2-} = 0), E5 (SO_4^{2-}:CO_3^{2-} = 0.96) and E8 (SO_4^{2-}:CO_3^{2-} = 1.62). All three spectra are characterized by strong bands in the ranges 1410–1500 cm^{-1}, 840–870 cm^{-1} and 700–750 cm^{-1}, which are characteristics of the carbonate ion vibrational modes in vaterite and calcite: 1490 (ν_3), 1085 and 1070 (ν_1), 870, 850 and 830 (ν_2) and 745 (ν_4), in vaterite; and 1430 (ν_3), 870 and 845 (ν_2) and 713 (ν_4) in calcite. Bands at 1130, 670, 628 and 608 cm^{-1}, which are absent in spectrum E0 (precipitate formed in the absence of dissolved sulfate), can be assigned to sulfate ions incorporated into the lattice of the $CaCO_3$ polymorphs.

supersaturation of the parental solution, which controls the phases that form at the initial stages of the crystallization process; and the dissolved sulfate content of the solution, which strongly influences the mineral evolution of the precipitates over time. When the reactants are mixed, the formation of $CaCO_3$ is instantaneous. At the very initial stage of the precipitation, the "nominal" supersaturation of the solution is exceedingly high for all $CaCO_3$ polymorphs ($SI_{calcite} \approx 3.74 \pm 0.04$; $SI_{aragonite} \approx 3.60 \pm 0.04$; $SI_{vaterite} \approx 3.17 \pm 0.04$). Under such conditions, the rapid formation of a most soluble and disordered phase such as vaterite is kinetically favored (Sawada, 1998), in agreement with the Ostwald step rule (Söhnel and Garside, 1992). It is noteworthy that other more soluble and disordered phases, like ACC, might form prior to vaterite, as reported by numerous authors (Addadi et al., 2003; Loste et al., 2003; Pontoni et al., 2003). Although neither the XRD nor the IR spectroscopic analyses showed any evidence of the presence of this phase in the precipitates, its presence in the very initial stages of the process cannot be dismissed. The higher reactivity and instability of this phase (Rodríguez-Blanco et al., 2008), together with the specific characteristics of our experimental set up, would preclude its detection.

After vaterite nucleation, the system remained supersaturated with respect to the other less soluble polymorphs. The formation of calcite nuclei allowed the system to further reduce its free energy, triggering a solvent-mediated transformation process (Cardew and Davey, 1985). This process should progress through the coupled dissolution of the more soluble vaterite and the growth of the less soluble calcite. As the system approaches equilibrium, thermodynamic factors predominate and no other $CaCO_3$ polymorph but calcite should remain in the system. Such an evolution occurs when the initial SO_4^{2-}:CO_3^{2-} ratio in the fluid is lower than one. However, as previously described, in solutions with SO_4^{2-}:CO_3^{2-} ratios higher than one, vaterite unexpectedly remains as a major constituent phase in the precipitate for long reaction periods, implying that the transformation of vaterite into calcite is much slower. Therefore, our results strongly suggest that a high SO_4^{2-}:CO_3^{2-} ratio in the initial solution inhibits this transformation and contributes to the stabilization of vaterite with respect to calcite.

The influence of SO_4^{2-} ions on calcite growth has been noted by several authors. For instance, Bischof and Fyfe (1968) and Bischof (1968) found that SO_4^{2-} ions both promote the formation of aragonite with respect to calcite and have a retarding or inhibiting effect on the transformation of vaterite into aragonite and of aragonite into calcite. Furthermore, the formation of metastable vaterite in nature and the presence of high concentrations of SO_4^{2-} ions in the crystallization media have been linked (Lippmann, 1973; Grasby, 2003). Recently, Fernández-Díaz et al. (2009) reported that the pseudomorphic carbonation of gypsum crystals in contact with stagnant Na_2CO_3 aqueous solutions involves the formation of different $CaCO_3$ polymorphs. These polymorphs sequentially transform into the more stable calcite via dissolution–crystallization, although such transformation is hindered when the SO_4^{2-}:CO_3^{2-} ratio in the fluid is higher than 1.3.

The influence of the SO_4^{2-}:CO_3^{2-} ratio in the crystallization medium on the evolution of the mineral composition of the precipitate must be related to the specific characteristics of the solids formed. The EDX analyses of the solids formed during the initial stages of crystallization (Fig. 4) show that both vaterite and calcite crystals incorporate sulfate in a proportion that linearly correlates with the initial SO_4^{2-}:CO_3^{2-} ratio in the fluid. Because the excitation depth of the electron in calcite and vaterite is on the order of ~2 μm (Long, 1995), and the particles' average diameter is ~10 μm, the compositional information provided by the EDX analyses can be considered representative of a significant percentage (⩾40%) of the particles' volume. The IR spectra of the vaterite and calcite precipitates (Fig. 5) are also consistent with the incorporation of sulfate ions in their structure. In the case of calcite, the formation of a limited $Ca(CO_3,SO_4)$ solid solution was proposed early on by Busenberg and Plummer (1985) on the basis of the XRD shift of *d*-spacings as a function of calcite sulfate content. Recently, the substitution of sulfate for carbonate groups in the calcite structure was corroborated by the application of synchrotron radiation-based techniques (Frisia et al., 2005).

Because the structures of calcite, aragonite and vaterite are different, the substitution of CO_3^{2-} groups by SO_4^{2-} will affect the free energy of these polymorphs differently, and, in turn, their relative stability. Computational modeling of the substitution of small percentages of CO_3^{2-} groups by SO_4^{2-} in the structures of calcite, aragonite and vaterite can provide information about how it affects their lattice energy and clues to the role of sulfate in the crystallization of $CaCO_3$.

3.2. Effects of the substitution CO_3^{2-}–SO_4^{2-} on the energy and geometry of the crystal structures of calcite, aragonite and vaterite

Fig. 6 shows the increments in the lattice energy (ΔE) of calcite, aragonite and vaterite doped with different amounts of sulfate relative to the corresponding pure phase. The proportion of sulfate incorporated into the crystal structure is expressed as the SO_4^{2-} mole% (% SO_4^{2-} in the figures). The bond energy accumulated by the CO_3^{2-} and SO_4^{2-} anions, which is different and characteristic of each anionic group, is included in the GULP calculations. To discount for this difference, as it is irrelevant to our purpose, the results were normalized with respect to equivalent mechanical mixtures of the corresponding pure phases of $CaCO_3$ (calcite, aragonite or vaterite) and $CaSO_4$ (anhydrite). It is noteworthy that the range of SO_4^{2-} concentration used in the calculations is consistent with that found in natural biogenic (Plummer and Busenberg, 1982) and inorganic (Wynn et al., 2010) samples.

As can be seen in Fig. 6, the data fit well to the linear functions in all three cases, for the range of compositions considered. In the case of calcite and aragonite, the substitution of carbonate by sulfate led to a positive increment of the lattice energy for the compositions explored. For equivalent compositions, the increment of lattice energy was always smaller for calcite (Fig. 6a) than for aragonite (Fig. 6b), indicating that the substitution was particularly unfavorable in the case of the aragonite structure.

The changes in crystal lattice energy reflect the degree of distortion that the calcite and aragonite structures suffered as a consequence of the substitution of CO_3^{2-} by SO_4^{2-}. Representative examples of the relaxed crystal structures of calcite and aragonite are shown in Fig. 7. In these super-cells, one carbonate group was substituted by one sulfate group. For clarity, only a region of about 15 Å around SO_4^{2-} is represented. In the case of calcite (Fig. 7a), the tetrahedral SO_4^{2-} group relaxed to a specific orientation in which three of the oxygen atoms were parallel to the CO_3^{2-} triangular groups of the crystal structure. This final relaxed orientation was always achieved, whatever the initial orientation of the sulfate group. The main distortion produced by the substitution of a sulfate group involves structural units located close to the apical oxygen of the sulfate anion, including a rotation of CO_3^{2-} groups and a displacement of the Ca^{2+} ions to accommodate the larger anion. In the case of aragonite (Fig. 7b), the substitution led to a significant distortion of the crystal structure, affecting mainly the CO_3^{2-} triangular groups located closer to the SO_4^{2-} anion, as a result of the repulsion forces between their oxygen atoms. Note that the distortion stretched beyond the two cells around the foreign sulfate group.

The results obtained for vaterite differ from the previous results. As mentioned above, for modeling the CO_3^{2-}–SO_4^{2-}

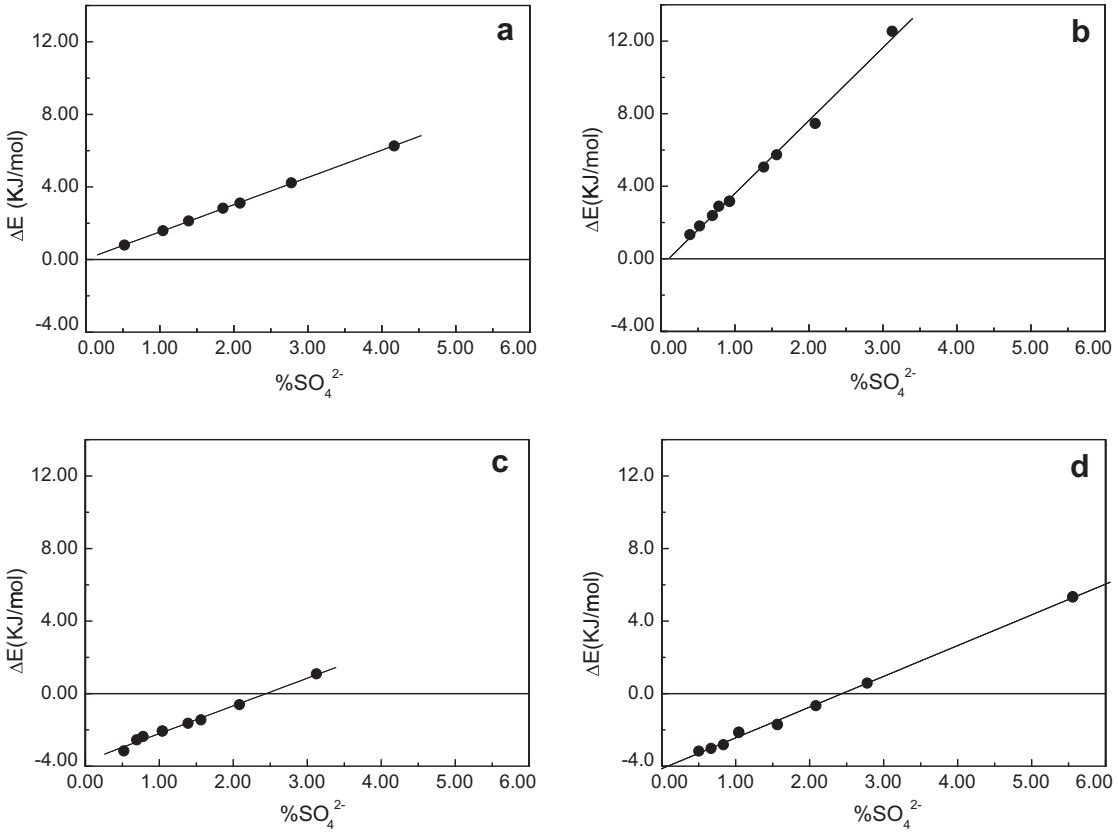

Fig. 6. Increment of energy (ΔE) in the crystal lattices of (a) calcite, (b) aragonite, (c) hexagonal vaterite and (d) orthorhombic vaterite as a function of sulfate content. The maximum mole percent of sulfate considered are 4.17 in calcite, 3.13 in aragonite, 5.56 in hexagonal vaterite and 3.13 in orthorhombic vaterite.

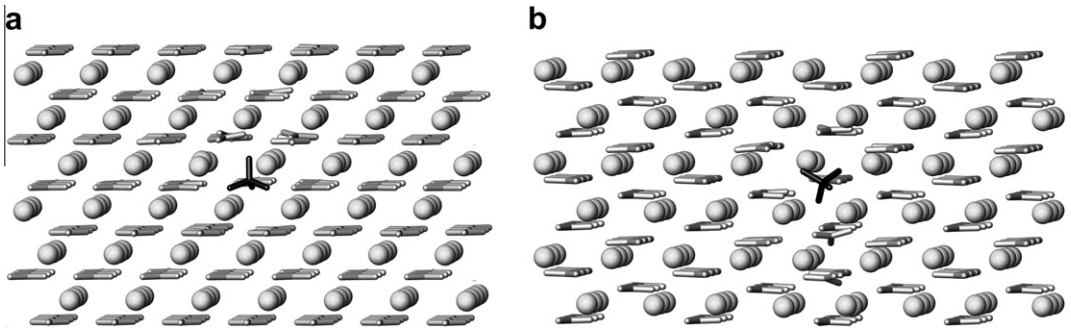

Fig. 7. Relaxed crystal structures of (a) calcite and (b) aragonite containing 0.5 mole% of sulfate.

substitution in vaterite, two strategies were followed. These strategies were based on using, respectively, the orthorhombic *Pbmn* structure (Meyer, 1960), which allows no CO_3^{2-} structural disorder, and the hexagonal $P6_3/mmc$ structure (Kamhi, 1963), in which the CO_3^{2-} groups are randomly distributed in three possible orientations. Both calculation methods provided similar results. The variation of ΔE as a function of SO_4^{2-} mole percent ($\%SO_4^{2-} < 6\%$) is depicted in Fig. 6c and d for the orthorhombic and hexagonal structural models, respectively. As can be seen, in both cases, the change in the lattice energy was negative for a wide range of substitutions ($\%SO_4^{2-} < 2$). Hence, the substitution of SO_4^{2-} for CO_3^{2-} was energetically much more favorable in the vaterite than in the calcite and aragonite. In fact, when the sulfate molar fraction was smaller than 2%, the doped vaterite was more stable than the pure vaterite because $\Delta E < 0$.

The distortion of the hexagonal vaterite structure caused by the substitution of a small fraction of CO_3^{2-} groups by SO_4^{2-} is depicted in Fig. 8, where images a, b and c represent the three possible carbonate group orientations. As can be observed, the SO_4^{2-} group relaxes to a position in which the S–O bonds tend to be parallel to the C–O bonds in the CO_3^{2-} groups. In this orientation, SO_4^{2-} mimics the arrangement of the carbonate groups, and the distortion of the structure is minimal.

The differential capacity of the three polymorphs to accommodate the SO_4^{2-} groups in the CO_3^{2-} lattice positions can be related to the different geometries of their structures. The substitution of a larger tetrahedron-shaped anion like SO_4^{2-} for a triangular group like CO_3^{2-} can be expected to be more difficult in the more densely packed crystal structures. Aragonite ($\rho = 2.93$ g/cm^3) is the densest polymorph, followed by calcite ($\rho = 2.73$ g/cm^3) and vaterite ($\rho = 2.66$ g/cm^3). The differential densities among the three polymorphs is consistent with the calculated changes in lattice energy following sulfate substitution. The high positive values of ΔE obtained for the sulfate-doped aragonite and calcite indicate that, in both cases, there was a clear tendency to un-mixing. Therefore, the sulfate-doped crystals can be expected to be less stable than the pure solids for the compositions considered. In contrast, in the case of vaterite, the incorporation of a small proportion of larger anions like sulfate seems to stabilize its low-density structure, as reflected by the negative values of ΔE obtained in our calculations.

3.3. Influence of sulfate concentration on the driving force of the vaterite–calcite transformation

The previous calculations account for the evolution observed in the precipitation experiments. In all cases, the initial precipitates consisted of vaterite and calcite. The metastable crystallization of vaterite can be explained by kinetic effects in response to the high supersaturation under which the precipitation occurred. Nevertheless, the subsequent evolution of the precipitates cannot be attributed exclusively to kinetic factors, but to a combination of thermodynamic and kinetic effects arising from the characteristics of these precipitates. The EDX chemical analysis of the calcite and vaterite crystals formed in the same experiment shows that the calcite was enriched in sulfate relative to the vaterite. Moreover, not only did the sulfate content of the precipitates increase with the SO_4:CO_3 ratio of the parent solutions but so did the difference between the two solid phases (see Fig. 4). According to our lattice energy model,

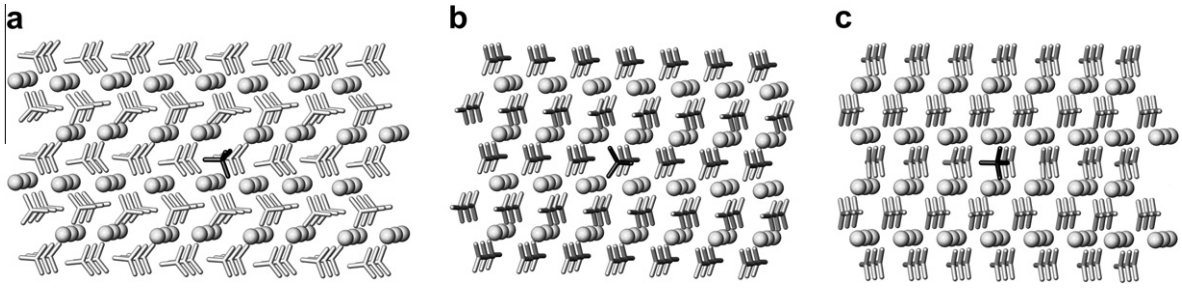

Fig. 8. Relaxed crystal structure of vaterite containing 0.7 mole% of sulfate. The three images (a), (b) and (c) represent the three possible orientation variants of vaterite.

the incorporation of sulfate stabilizes the vaterite structure but destabilizes the calcite structure. Consequently, the driving force for the transformation of vaterite into calcite decreases with the sulfate content in the initial solution. This decrease is depicted in Fig. 9, where the difference between the increment of the lattice energy (Fig. 6) of the coexisting calcite and the vaterite in experiments E0–E8 ($\Delta E_{vat}-\Delta E_{cal}$), according to their S content (Fig. 4), is plotted against the SO_4^{2-}:CO_3^{2-} mole ratio in the initial solution. The driving force for the vaterite–calcite transformation is proportional to (ΔE_{vat}–ΔE_{cal}) and, hence, decreases with the sulfate content in the solution. The final outcome is that vaterite, the $CaCO_3$ polymorph whose structure best accommodates sulfate groups, persists a longer time (its relative stability increases) when the sulfate concentration in the initial solution increases. Although the influence of sulfate ion adsorption on the vaterite and calcite surfaces cannot be ruled out, in the present experiments, the lattice substitution of sulfate for carbonate groups can be considered the most relevant factor affecting the rate of re-crystallization.

The observed behavior is consistent with the fact that the solubility of solid solutions varies with composition (Glynn and Reardon, 1990; Prieto et al., 1997). Busenberg and Plummer (1985) experimentally measured the solubility of calcites containing different amounts of SO_4^{2-}. They found that the solubility of calcites containing up to $\approx$ 1 mole% SO_4^{2-} is slightly less to equally soluble than pure calcite. Conversely, calcites with higher SO_4^{2-} contents ($\Delta E_{cal} > 0$) are more soluble than pure calcite, whereas calcites containing more than 3 mole% SO_4^{2-} are more soluble than pure aragonite (Busenberg and Plummer, 1985). In contrast to the calcite behavior, according to the lattice energy calculations, the incorporation of sulfate into vaterite is expected ($\Delta E_{vat} < 0$) to decrease its solubility. Because of the differential solubility behavior of sulfate-doped calcite and vaterite, their solubilities will converge as their sulfate content increases. The immediate consequence is a reduction of the driving force (directly related to the difference in solubility) for the solvent-mediated transformation of vaterite into calcite. Thus, the increase in the sulfate content of both phases with the initial SO_4^{2-}:CO_3^{2-} ratio in the fluid explains the slower transformation when this ratio is increased.

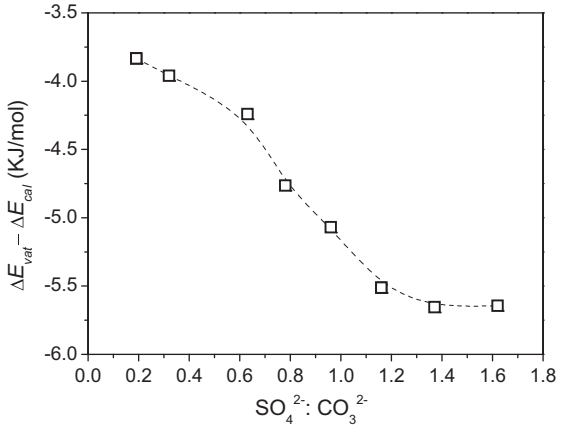

Fig. 9. Difference $\Delta E_{vat}-\Delta E_{cal}$ between the increment of lattice energy corresponding to the "sulfate-bearing" vaterite and calcite crystals obtained in experiments E1–E8 as a function of the SO_4^{2-}:CO_3^{2-} mole ratio in the initial solution.

The result of our calculation, showing that the substitution of sulfate for carbonate groups into aragonite is less favourable than into calcite, may appear in conflict with the conclusion from Bischoff's experiments (Bischof, 1968; Bischof and Fyfe, 1968) in which sulfate inhibits the aragonite to calcite transformation. In fact, our computational results provide a suitable explanation for the results of Bischoff's experiments, in which seeds of "pure" aragonite were maintained in contact with aqueous solutions containing sulfate. The driving force for the solvent-mediated transformation of aragonite into calcite would be determined by the difference in solubility between the original pure aragonite phase (the seeds introduced in the system) and a calcite that would nucleate from the sulfate-bearing aqueous solution and presumably incorporate some sulfate in its structure. As previously discussed, the solubility of such a sulfate-bearing calcite ($\Delta E_{cal} > 0$) would be very close to that of pure aragonite, or even higher if the sulfate content of the calcite is significant (Busenberg and Plummer, 1985). Under these conditions, the driving force for the transformation would be very small to negligible. As a result, aragonite would transform into calcite at a very low rate or would not transform at all.

4. CONCLUDING REMARKS

The experiments presented above illustrate the mineralogical evolution of calcite and vaterite precipitates formed from aqueous solutions that are highly supersaturated with respect to $CaCO_3$ phases and that contain increasing SO_4^{2-}:CO_3^{2-} molar ratios. When the SO_4^{2-}:CO_3^{2-} ratio in the parental fluid was $\leqslant$1, the vaterite rapidly transformed into calcite. In contrast, vaterite persisted as a major phase-component of the precipitate when the initial solutions were SO_4^{2-}:$CO_3^{2-} \geqslant 1$. The progressively more sluggish kinetics of this solvent-mediated transformation with increasing sulfate content can be related to changes in the solubility of the two solid phases due to the lattice substitution of sulfate for carbonate groups in their structures. The computational modeling shows that a certain degree of substitution (<3%) is energetically favorable in the case of vaterite, unfavorable in calcite and even more unfavorable in aragonite. Our calculations also give a reasonable explanation for the results of previous seeded experiments in addition to providing thermodynamic support to the natural occurrences of vaterite in evaporitic deposits, where the formation of $CaCO_3$ takes place in the presence of high sulfate ion concentrations in the crystallization media (Grasby, 2003).

ACKNOWLEDGMENTS

Financial support through the Spanish Ministry of Science and Innovation (Project CGL2007-65523-C02-01 and -02) and the Comunidad de Madrid (Project CAM-2009 910148) is gratefully acknowledged. We sincerely thank the staff from the Microscopy Centre-UCM for assistance and support with the SEM, the staff

from the X-ray Diffraction Central Service-UCM for assistance and technical support, Dr. Emilio Matesanz for help with the XRD interpretation and Pedro Rodríguez Pascual, from the Material Science Institute of Madrid (CSIC), for technical support with the FTIR spectroscopy. We acknowledge the Barcelona Supercomputing Center (Centro Nacional de Supercomputación) for providing access to the MareNostrum Supercomputer. The authors wish to thank Michael Böttcher and two anonymous reviewers for helpful comments. The thorough review and editing of the manuscript provided by Alfonso Mucci are gratefully acknowledged.

REFERENCES

Adam C. D. (2003) Atomistic modelling of the hydration of $CaSO_4$. *J. Solid Stat. Chem.* **174**, 141–151.

Addadi L., Raz S. and Weiner S. (2003) Taking advantage of disorder: amorphous calcium carbonate and its roles in biomineralization. *Adv. Mater.* **15**, 959–970.

Aizenberg J., Lambert G., Weiner S. and Addadi L. (2002) Factors involved in the formation of amorphous and crystalline calcium carbonate: a study of an ascidian skeleton. *J. Am. Chem. Soc.* **124**, 32–39.

Aizenberg J., Weiner S. and Addadi L. (2003) Coexistence of amorphous and crystalline calcium carbonate in skeletal tissues. *Connect. Tissue Res.* **44**, 20–25.

Allan N. L., Rohl A. L., Gay D. H., Catlow R. A., Davey R. J. and Mackrodt W. C. (1993) Calculated bulk and surfaces properties of sulfates. *Faraday Discuss.* **95**, 273–280.

Becker U., Risthaus P., Brandt F. and Bosbach D. (2006) Thermodynamic properties and crystal growth behavior of the hashemite ($BaSO_4$–$BaCrO_4$) solid solution. *Chem. Geol.* **225**, 244–255.

Beniash E., Aizenberg J., Addadi L. and Weiner S. (1997) Amorphous calcium carbonate transforms into calcite during sea urchin larval spicule growth. *Proc. R. Soc. B. Biol. Sci.* **264**, 461–465.

Bensted J. (1976) Characterization of sulphate bands in the IR-spectra of minerals. *Naturwissenschaften* **63**, 193.

Bischof J. L. (1968) Catalysis, inhibition, and the calcite–aragonite problem. I. The vaterite–aragonite transformation. *Am. J. Sci.* **266**, 65–79.

Bischof J. L. and Fyfe W. S. (1968) Catalysis, inhibition, and the calcite–aragonite problem. II. The aragonite–calcite transformation. *Am. J. Sci.* **266**, 80–90.

Bolze J., Peng B., Dingenouts N., Panine P., Narayanan T. and Ballauff M. (2002) Formation and growth of amorphous colloidal $CaCO_3$ precursor particles as detected by time-resolved SAXS. *Langmuir* **18**, 8364–8369.

Born M. and Huang K. (1954) *Dynamical theory of crystal lattices*. Oxford University Press, Oxford, UK.

Bruno M., Massaro F. R. and Prencipe M. (2008) Theoretical structure and surface energy of the reconstructed 01.2 form of calcite ($CaCO_3$) crystal. *Surf. Sci* **602**, 2774–2782.

Busenberg E. and Plummer N. (1985) Kinetic and thermodynamic factors controlling the distribution of SO_4^{2-} and Na^+ in calcites and selected aragonites. *Geochim. Cosmochim. Acta* **49**, 713–725.

Cardew P. T. and Davey R. J. (1985) The kinetics of solvent-mediated phase transformations. *Proc. R. Soc. London A* **398**, 415–428.

Chen S. F., Yu S. H., Jiang J., Fanquing L. and Yankuan L. (2006) Polymorph discrimination of $CaCO_3$ mineral in an ethanol/water solution: Formation of complex vaterite superstructures and aragonite rods. *Chem. Mater.* **18**, 115–122.

Chernov A. A. (1970) Growth of copolymer chains and mixed crystals-trial-and-error statistics. *Sov. Phys. Usp. USSR* **13**, 101.

Cusack M., Dauphin Y., Cuif J. P., Salomé M., Freer A. and Yin H. (2008) Micro-XANES mapping of sulphur and its association with magnesium and phosphorus in the shell of the brachiopod, Terebratulina retusa. *Chem. Geol.* **253**, 172–179.

de Leeuw N. H. and Parker S. C. (1998) Surface structure and morphology of calcium carbonate polymorphs calcite, aragonite, and vaterite: an atomistic approach. *J. Phys. Chem. B* **102**, 2914–2922.

de Villiers J. P. R. (1971) Crystal structures of aragonite, strontianite, and witherite. *Am. Mineral.* **56**, 758–767.

Farmer V. C. (1974) *The Infrared spectra of minerals*. Mineralogical Society.

Fernández-Díaz L., Putnis A., Prieto M. and Putnis C. V. (1996) The role of magnesium in the crystallization of calcite and aragonite in a porous medium. *J. Sed. Res.* **66**, 482–491.

Fernández-Díaz L., Pina C. M., Astilleros J. M. and Sánchez-Pastor N. (2009) The carbonatation of gypsum: pathways and pseudomorph formation. *Am. Mineral.* **94**, 1223–1234.

Fernández-González A., Pedreira V. B. and Prieto M. (2008) Crystallization of zoned (Ba,Pb)SO_4 single crystals from aqueous solutions in silica gel. *J. Cryst. Growth* **310**, 4616–4622.

Fleming S. and Rohl A. (2005) GDIS: a visualization program for molecular and periodic systems. *Z. Kristall.* **220**(5–6), 580–584.

Frisia S., Borsato A., Fairchild I. J. and Susini J. (2005) Variations in atmospheric sulfate recorded in stalagmites by synchrotron micro-XRF and XANES analyses. *Earth Planet. Sci. Lett.* **235**, 729–740.

Gale J. D. (1997) GULP: a computer-program for the symmetry-adapted simulation of solids. *J. Chem. Soc. Faraday Trans.* **93**, 629–637.

Gale J. D. and Rohl A. L. (2003) The general utility lattice program. *Mol. Simul.* **29**, 291–341.

Giuseppetti G., Mazzi F. and Tadini C. (1998) The crystal structure of synthetic burkeite $Na_4SO_4(CO_3)_t(SO_4)_{1-t}$. *N. Jahrb. Mineral. Monats.* **1988**(5), 203–221.

Glynn P. D. and Reardon E. J. (1990) Solid solution–aqueous solution equilibria: thermodynamic theory and representation. *Am. J. Sci.* **290**, 164–201.

Graf D. L. (1961) Crystallographic tables for the rhombohedral carbonates. *Am. Mineral.* **46**, 1283–1316.

Grasby S. E. (2003) Naturally precipitating vaterite (μ-$CaCO_3$) spheres: unusual carbonates formed in an extreme environment. *Geochim. Cosmochim. Acta* **67**, 1659–1666.

Griesshaber E., Kelm K., Sehrbrock A., Mader W., Mutterlose J., Brand U. and Schmahl W. W. (2009) Amorphous calcium carbonate in the shell material of the brachiopod Megerlia truncate. *Eur. J. Mineral.* **21**, 715–723.

Hadiko G., Han Y. S., Fuji M. and Takahashi M. (2005) Synthesis of hollow calcium carbonate particles by the bubble templating method. *Mater. Lett.* **59**, 2519–2522.

Hanor J. S. (2004) A model for the origin of large carbonate- and evaporate-hosted celestine ($SrSO_4$) deposits. *J. Sed. Res.* **74**, 168–175.

Hasse B., Ehrenberg H., Marxen J. C., Becker W. and Epple M. (2000) Calcium carbonate modifications in the mineralized shell of the freshwater snail Biomphalaria glabrata. *Chem. Eur. J.* **6**, 3679–3685.

House W. A. (1987) Inhibition of calcite growth by inorganic phosphate. *J. Colloid Interface Sci.* **119**, 505–511.

Ito T. (1996) Ikaite from cold spring water at Shiowakka, Japan. *J. Min. Pet. Econ. Geol.* **91**, 209–219.

Kamhi S. R. (1963) On the structure of vaterite, $CaCO_3$. *Acta Cryst.* **16**, 770–772.

Katsikopoulos D., Fernández-González A. and Prieto M. (2009) Precipitation and mixing properties of the "disordered" (Mn, Ca)CO_3 solid solution. *Geochim. Cosmochim. Acta* **73**, 6147–6161.

Kile D., Eberl D. D., Hoch A. R. and Reddy M. M. (2000) An assessment of calcite crystal growth mechanisms based on crystal size distributions. *Geochim. Cosmochim. Acta* **64**, 2937–2950.

Kitamura M. (2002) Controlling factor of polymorphism in crystallization process. *J. Cryst. Growth* **237–239**, 2205–2214.

Kowacz M., Prieto M. and Putnis A. (2010) Kinetics of crystal nucleation in ionic solutions: electrostatics and hydration forces. *Geochim. Cosmochim. Acta* **74**, 469–481.

Land L. S. and Hoops G. K. (1973) Sodium in carbonate sediments and rocks: a possible index to salinity of diagenetic solutions. *J. Sed. Petrol.* **43**, 614–617.

Larsen D. (1994) Origin and Paleoenvironmental Significance of calcite pseudomorphs after ikaite in the Oligocene Creede Formation. *Colorado. J. Sed. Res.* **64**, 593–603.

Lippmann F. (1973) *Sedimentary Carbonate Minerals*. Springer-Verlag.

Long V. P. (1995) Microanalysis from 1950 to the 1990s. In *Microprobe Techniques in the Earth Sciences* (eds. P. J. Potts, J. F. W. Bowles, S. J. B. Reed and M. R. Cave). Chapman and Hall, London, pp. 1–48.

Loste E., Wilson R. M., Seshadri R. M. and Meldrum F. C. (2003) The role of magnesium in stabilising amorphous calcium carbonate and controlling calcite morphologies. *J. Cryst. Growth* **254**, 206–218.

Medeiros S. K., Albuquerque E. L., Maia, Jr., F. F., Caetano E. W. S. and Freire V. N. (2007) First-principles calculations of structural, electronic, and optical absorption properties of $CaCO_3$ Vaterite. *Chem. Phys. Lett.* **435**, 59–64.

Meldrum F. C. (2003) Calcium carbonate in biomineralisation and biomimetic chemistry. *Int. Mater. Rev.* **48**, 187–224.

Meyer H. J. (1960) Vaterite and its structure. *Fortschr. Mineral.* **38**, 186–187.

Nebel H. and Epple M. (2008) Continuous preparation of calcite, aragonite and vaterite, and of magnesium-substituted amorphous calcium carbonate (Mg-ACC). *ZAAC* **634**(8), 1439–1443.

Ogino T., Suzuki T. and Sawada K. (1987) The formation and transformation mechanism of calcium carbonate in water. *Geochim. Cosmochim. Acta* **51**, 2757–2767.

Park S. K. and Miller K. W. (1988) Random number generators: good ones are hard to find. *Comm. Assoc. Comput. Mach.* **31**, 1192–1201.

Parkhurst D. L. and Appelo C. A. J. (1999) User's Guide to PHREEQC, US Geological Survey *Water Resources Investigations Report* **99–4259**, US Geological Survey, Washington, DC.

Pingitore N. E., Meitzner G. Jr. and Love K. M. (1995) Identification of sulfate in natural carbonates by X-ray absorption spectroscopy. *Geochim. Cosmochim. Acta* **59**, 2477–2483.

Plummer L. N. and Busenberg E. (1982) The solubilities of calcite, aragonite and vaterite in CO_2–H_2O solutions between 0 and 90 °C, and an evaluation of the aqueous model for the system $CaCO_3$–CO_2–H_2O. *Geochim. Cosmochim. Acta* **46**, 1011–1040.

Pontoni D., Bolze J., Dingenouts N., Narayanan T. and Ballauff M. (2003) Crystallisation of calcium carbonate observed in-situ by combined small and wide angle X-ray scattering. *J. Phys. Chem. B* **107**, 5123–5125.

Prieto M., Fernández-González A., Putnis A. and Fernández-Díaz L. (1997) Nucleation, growth, and zonning phenomena in crystallizing (Ba,Sr)CO_3, Ba(SO_4,CrO_4), (Ba,Sr)SO_4, and (Cd,Ca)CO_3 solid solutions from aqueous solutions. *Geochim. Cosmochim. Acta* **61**, 3383–3397.

Prieto M., Becker U., Fernández-González A. and Putnis A. (2000) Computing Lippmann diagrams from direct calculation of mixing properties of solid solutions: application to the barite–celestite system. *Aquat. Geochem.* **6**, 133–146.

Reddy M. M. and Nancollas G. H. (1976) The crystallization of calcium carbonate. IV. The effect of magnesium, strontium and sulfate ions. *J. Cryst. Growth* **35**, 33–38.

Reddy M. M. and Wang K. K. (1980) Crystallization of calcium carbonate in the presence of metalions. Inhibition by magnesium ion at pH 8.8 and 25 °C. *J. Cryst. Growth* **50**, 470–480.

Rodríguez-Blanco J. D., Shaw S. and Benning L. G. (2008) How to make stable "ACC": control and preliminary characterization? *Miner. Mag.* **72**, 283–286.

Rohl A. L., Wright K. and Gale J. D. (2003) Evidence from surface phonons for the (2x1) reconstruction of the (1014) surface of calcite from computer simulation. *Am. Mineral.* **88**, 921–925.

Sangwal K. (2007) *Additives and Crystallization Processes: From Fundamentals to Applications.* Wiley.

Sawada (1998) Mechanisms of crystal growth of inonic crystals in solution. Formation, transformation, and growth inhibition of calcium carbonates. In *Crystallization Processes* (ed. H. Ohtaki). Wiley.

Schulz H. D. and Zabel M. (2007) *Marine Geochemistry*. Springer.

Smith A. M. L., Hudson-Edwards K. A., Dubbin W. E. and Wright K. (2006) Defects and impurities in jarosite: a computer simulation study. *Appl. Geochem.* **21**, 1251–1258.

Snyder R. L. (1992) The use of reference intensity ratios in X-ray quantitative analysis. *Powder Diffr.* **7**, 186–193.

Söhnel O. and Garside J. (1992) *Precipitation*. Butterworth-Heinemann, Oxford.

Söhnel O. and Mullin J. W. (1987) Interpretation of crystallization induction periods. *J. Colloid Interface Sci.* **123**, 43–50.

Titiloye J. O., Parker S. C. and Mann S. (1993) Atomistic simulation of calcite surfaces and the influence of growth additives on their morphology. *J. Cryst. Growth* **131**, 533–545.

Titiloye J. O., de Leeuw N. H. and Parker S. C. (1998) Atomistic simulation of the differences between calcite and dolomite surfaces. *Geochim. Cosmochim. Acta* **62**, 2637–2641.

Tokuyama A., Kitano Y. and Kaneshima K. (1972) Geochemical behaviour of chemical species in the processes of limestones formation. Part 1. Chemical compositions of corals and limestones in the Tyuku Islands. *Geochem. J.* **6**, 83–92.

Vagenas N. V., Gatsouli A. and Kontoyannis C. G. (2003) Quantitative analysis of synthetic calcium carbonate polymorphs using FT-IR spectroscopy. *Talanta* **59**, 831–836.

Weiner S. and Dove P. M. (2003) An overview of biomineralization processes and the problem of vital effect. *Rev. Mineral. Geochem.* **54**, 1–31.

Wynn P. M., Fairchild I. J., Frisia S., Spötl C., Baker A. and Borsato A.EIMF (2010) High-resolution sulphur isotope analysis of speleothem carbonate by secondary ionisation mass spectrometry. *Chem. Geol.* **271**, 101–107.